^{99m}Tc-$(CO)_3$ His-Annexin A5 Micro-SPECT Demonstrates Increased Cell Death by Irinotecan During the Vascular Normalization Window Caused by Bevacizumab

Christel Vangestel[1], Christophe Van de Wiele[2], Nancy Van Damme[3], Steven Staelens[4], Patrick Pauwels[5], Chris P.M. Reutelingsperger[6], and Marc Peeters[1,7]

[1]Department of Gastroenterology, Ghent University Hospital, Ghent, Belgium; [2]Department of Nuclear Medicine and Radiology, Ghent University Hospital, Ghent, Belgium; [3]Department of Surgery, Ghent University Hospital, Ghent, Belgium; [4]Department of Nuclear Medicine, Molecular Imaging Centre Antwerp, University of Antwerp, Antwerp, Belgium; [5]Department of Pathology, University Hospital Antwerp, Antwerp, Belgium; [6]Department of Biochemistry, Cardiovascular Research Institute, University of Maastricht, Maastricht, The Netherlands; and [7]Department of Oncology, University Hospital Antwerp, Antwerp, Belgium

Colorectal tumors are dependent on angiogenesis for growth, and vascular endothelial growth factor (VEGF) is a key mediator of tumor angiogenesis. Antiangiogenic drugs can induce a transient normalization of the tumor vasculature with improved delivery of coadministered chemotherapy. The efficacy of antihuman VEGF antibody (bevacizumab) with or without irinotecan was evaluated in a colorectal cancer xenograft using ^{99m}Tc-$(CO)_3$ His-annexin A5. **Methods:** Colo205-bearing mice were treated with a single dose of bevacizumab (5 mg/kg) during 2, 4, or 6 d. Microvessel density, pericyte coverage (α-smooth-muscle actin immunostaining), collagen-covered tumor vessels (Masson trichrome staining), and tumor hypoxic fraction (pimonidazole staining) were determined at the 3 different time points after treatment with bevacizumab. To investigate the possible synergistic effects of combination therapy with bevacizumab and irinotecan, Colo205-bearing mice were treated with a single dose of bevacizumab 2, 4, or 6 d before administration of a single dose of irinotecan (100 mg/kg) or 0.9% NaCl. The apoptosis-detecting radiotracer ^{99m}Tc-$(CO)_3$ His-annexin A5 was injected (18.5 MBq) in mice 12, 24, and 48 h after the start of the irinotecan or NaCl treatment, and micro-SPECT was subsequently performed 3.5 h after injection of the radiotracer. Results were correlated to histologic analysis for apoptosis (caspase-3 activation). **Results:** Four days after bevacizumab administration, microvessel density decreased significantly, and α-smooth-muscle actin and collagen-covered vessels, compared with control tumors, were increased, suggesting normalization of the tumor vasculature. Hypoxic fraction was slightly reduced 4 d after treatment with bevacizumab. SPECT analyses demonstrated a significant increase in tumoral ^{99m}Tc-$(CO)_3$ His-annexin A5 uptake 4 d after bevacizumab treatment and 24 h after irinotecan administration (232.78 $\pm$ 24.82 percentage injected dose/tumor weight [g]/body weight [kg], $P < 0.05$), compared with each monotherapy, indicating a synergistic effect of both therapies. **Conclusion:** ^{99m}Tc-$(CO)_3$ His-annexin A5 micro-SPECT demonstrates increased antitumor activity of irinotecan during the transient vascular normalization period caused by bevacizumab. Our data outline the importance of timing of combined anti-VEGF treatment with chemotherapy.

Key Words: anti-VEGF; vascular normalization; chemotherapy delivery; ^{99m}Tc-$(CO)_3$ His-annexin A5; colorectal cancer

J Nucl Med 2011; 52:1786–1794
DOI: 10.2967/jnumed.111.092650

Little fundamental progress has been achieved in colorectal cancer (CRC) chemotherapy the past 20 y, and attention has been shifted to antiangiogenic therapies. Bevacizumab (Avastin; Genetech/Roche) is a humanized monoclonal antibody that targets and inhibits vascular endothelial growth factor (VEGF), a proangiogenic cytokine secreted by endothelial and malignant cells. Bevacizumab neutralizes all human isoforms of VEGF-A, inhibiting VEGF-induced proliferation of endothelial cells, and consequently suppresses tumor growth (*1,2*). Bevacizumab in combination with conventional chemotherapy significantly increases overall survival or progression-free survival in metastatic colorectal cancer patients (*3*). However, as the survival benefits of antiangiogenic drugs have been rather modest, there still remains an increasing interest in developing more effective ways to combine antiangiogenic drugs with conventional treatments.

The vasculature established in tumors is generally dysfunctional, with vessels that are tortuous, dilated, and leaky, leading to heterogeneous perfusion of the tumor. Pericytes are loosely attached to endothelial cells (or absent), and basement membrane is often abnormal (unusually thick or absent), leading to a typical tumor microenvironment. Elevated interstitial pressure, hypoxia, and acidosis interfere with the delivery and the cytotoxic effects

Received May 2, 2011; revision accepted Aug. 17, 2011.
For correspondence or reprints contact: Vangestel Christel, Ghent University Hospital, Department of Gastroenterology, De Pintelaan 185, 9000-B Ghent, Belgium.
E-mail: christel.vangestel@uza.be

of chemotherapy (*4*). According to the Jain hypothesis, treatment with bevacizumab can primarily improve chemotherapy efficacy by normalizing tumor vasculature, leading to a more effective oxygen and drug delivery (*5*). However, this normalization window is transient, and optimal timing of bevacizumab administration before chemotherapy delivery should be determined. Moreover, determination of this normalization window noninvasively is of great importance.

In the present study, we explore the effects of bevacizumab on the tumoral vasculature in a colorectal cancer xenograft, specifically on vessel density and morphology, vasculature maturation, tumor hypoxia, and chemotherapy (irinotecan) delivery. To image apoptotic tumor response induced by irinotecan (thus to demonstrate differential chemotherapy delivery to known tumor sites), ^{99m}Tc-$(CO)_3$ His-annexin A5 micro-SPECT was performed at different time points after bevacizumab administration before a single dose of irinotecan. Levels of VEGF-A in the tumor and serum were examined by enzyme-linked immunosorbent assay (ELISA), and transcription of genes involved in angiogenesis was assessed by quantitative polymerase chain reaction (PCR).

We previously validated the radiotracer ^{99m}Tc-$(CO)_3$ His-annexin A5 for apoptosis imaging in vitro and in vivo (including a biodistribution and dosimetric study), and early time course of cell death induced by a single dose of irinotecan and bevacizumab as monotherapy was demonstrated (*6,7*).

MATERIALS AND METHODS

Human Colorectal Cancer Xenograft Model

Colo205 cells (ATCC-CCL-222; American Type Culture Collection) were kept in culture as previously described (*6,7*). Female CD-1 nude mice, obtained from Charles River Inc. (strain code 086), were purchased at the age of up to 42 d and treated in accordance with Belgian regulation and animal experiments as approved by the local ethics committee. For the Colo205-bearing mouse model, mice were injected subcutaneously in the right hind leg with 1×10^6 Colo205 cells in a volume of 100 μL, as previously described (*6,7*). Because of our study design for the SPECT scans—the use of different animals at the different time points (to obtain tumor specimens at all time points)—longitudinal tumor growth curves cannot be obtained. However, tumor volumes were measured using a Vernier caliper and calculated with the ellipsoid formula $V = 1/2\ ab^2$, where a and b are the long and short axes of the tumor, respectively. Tumor volumes were measured at baseline (before bevacizumab administration) and at the different time points at the end of the experiment (12, 24, or 48 h after irinotecan or NaCl administration).

Study Design

Eighty-one mice were included for analysis. One group of 15 mice was used for bevacizumab monotherapy (5 mg/kg), receiving a single dose of bevacizumab (5 mg/kg) for 2 d (day 2), 4 d (day 4), or 6 d (day 6) ($n = 5$ in each time group). Twelve mice served as control and were sacrificed. The animals were killed by cervical dislocation, and tumors were removed. One third of the tumor was formalin-fixed and paraffin-embedded (histopathology), one third was snap-frozen and stored at −80°C (ELISA analysis), and one third was stored in RNAlater (Qiagen) at −80°C (quantitative PCR analysis).

One group of 54 mice was used for ^{99m}Tc-$(CO)_3$ His-annexin A5 SPECT scans. Mice were divided into 2 different groups: group 1 received a single dose of bevacizumab (5 mg/kg) at 2, 4, or 6 d before receiving a single dose of 0.9% NaCl, and group 2 received a single dose of bevacizumab at 2, 4, or 6 d before receiving a single dose of irinotecan (100 mg/kg). SPECT scans were obtained 12, 24, and 48 h after the start of the irinotecan (or 0.9% NaCl) treatment ($n = 3$ at each time point). Drugs were administered intraperitoneally. Control mice ($n = 9$) receiving a single injection of 0.9% NaCl underwent SPECT scans at 12, 24, and 48 h after administration of the NaCl. ^{99m}Tc-$(CO)_3$ His-annexin A5 SPECT scans of single-dose irinotecan (100 mg/kg) and bevacizumab (5 mg/kg) in Colo205-bearing mice were previously acquired (*7*).

^{99m}Tc-$(CO)_3$ His-Annexin A5 Preparation

^{99m}Tc-$(CO)_3$ His-annexin A5 was prepared as previously described (*6*). His-annexin A5 was kindly provided by Prof. Dr. Chris Reutelingsperger (Cardiovascular Research Institute). The radiochemical purity of the ^{99m}Tc-$(CO)_3$ His-annexin A5 was determined by ascending instant-thin layer chromatography with silica gel–coated fiberglass sheets (Life Sciences, Pall Corp.), as previously described (*6*). Radiochemical purities of 95% or greater and specific radioactivities of approximately 5,180–5,920 MBq of protein per μg were obtained for ^{99m}Tc-$(CO)_3$ His-annexin A5.

Micro-SPECT of Cell Death in Colo205-Bearing Mice

For in vivo imaging of apoptosis, Colo205-bearing mice were injected via a tail vein with 18.5 MBq of ^{99m}Tc-$(CO)_3$ His-annexin A5 at 12, 24, and 48 h after the start of the irinotecan (or 0.9% NaCl) treatment ($n = 3$ at each time point). Three and a half hours after injection of the radiotracer, mice were positioned in the scanner and were maintained under isoflurane anesthesia for the duration of the experimental procedure while body temperature was kept constant by a heating bed. Static high-resolution tomographic images were acquired in 4 frames of 5 min, with a focus on the tumor using the U-SPECT-II (Milabs). This micro-SPECT scanner is among several others equipped with a rat collimator consisting of a tungsten cylinder with 5 rings of 15-pinhole apertures (1.0-mm diameter) delivering reconstructed images with an iterative resolution better than 1 mm (*8*). All pinholes focused on a single volume in the center of the tube. For this study, the animal bed was translated in 3 dimensions using an *XYZ* stage into 2 different bed positions focused on the tumor. A 20% main photopeak was centered at 140 keV to reconstruct the ^{99m}Tc images on 0.75 mm^3 voxels by 6 iterations of 16 subsets (ordered-subsets expectation maximization). A syringe with a known amount of radioactivity was scanned along with the mice to allow semiquantification of the results. Region-of-interest (ROI) analysis and quantification of ^{99m}Tc-$(CO)_3$ His-annexin A5 accumulation were performed in PMod Software (PMOD Technologies). All tumors showed visible radiotracer uptake, and ROIs were drawn manually around the tumor on all consecutive slices encompassing the tumor. When defining the tumor ROIs, particular care was taken to avoid inclusion of any erroneous signal originating from the bladder. For the purpose of quantification, tumor lesion counts in tomographic slices were summed, thus incorporating the entire dimension of the tumor. Percentage uptake was obtained using the following equation: (total lesion radioactivity counts at time of SPECT × radioactivity of standard at time of SPECT scan/standard counts at time of SPECT × total radioactivity injected) × 100% and normalized to tumor weight (g) and body weight (kg).

Data from the SPECT scans are normalized to the control group of the same time point: mean percentage injected dose (%ID)/g/kg of the treated animals/mean %ID/g/kg of the control mice × 100%.

Immunostaining and Masson Trichrome Staining (Collagen Staining)

Sections (4 μm thick) were mounted on SuperFrost microscope slides (Menzel-Glaser), which were deparaffinized in xylene and rehydrated in a downgraded series of ethanol. Immunostaining of caspase-3, von Willebrand factor (vWF), and α-smooth-muscle actin (α-SMA; pericyte coverage) was performed according to the manufacturer's instruction. The appropriate primary and secondary antibodies with their corresponding dilution factors and incubation time, antigen retrieval, and visualization system are indicated in Supplemental Table 1 (supplemental materials are available online only at http://jnm.snmjournals.org). The color reaction was developed using the chromogen 3 3-diaminobenzidine+ (Dako) for 10 min. The tissue sections were counterstained with Mayer hematoxylin. Tris-buffered saline with Tween/5% normal goat serum or isotype control instead of the primary antibody was used as negative control.

The number of caspase-3–positive (apoptotic) cells present in each tumor specimen was expressed as a fraction of the total number of cells. The apoptotic index was determined using an Optronicscolor digital camera (Olympus Corp.) and specialized software (Cell D Olympus Imaging Solutions). Ten ROIs were chosen at random at a magnification of ×200. Highly necrotic regions were excluded from analysis.

To assess microvessel density (MVD) and positive α-SMA immunostaining, all the slides were scanned at low magnification (×100), and 5 vascular hot spots (areas with the highest vascularization) were determined. These 5 hot spots were digitally photographed at ×200, and positive staining was then quantified with cell^D imaging software (Olympus) and reported as the percentage positive staining per ×200 high-power field (0.38 mm^2). In all of the samples, the mean value of vWF- or α-SMA–positive areas was calculated from 5 vascular hot spots. Vessel maturity index (VMI) was calculated as the ratio of α-SMA to vWF staining. Masson trichrome staining was applied to assess the collagen around tumor vessels. Microvessels in the tumors, indicated by red blood cells, were counted, and the percentage of vessels surrounded by more and less than 50% collagen was calculated.

Staining of Tumor Hypoxia

To detect tumor hypoxia, pimonidazole (60 mg/kg) was injected intraperitoneally 1 h before mice were sacrificed. The Hypoxyprobe-1 kit (Chemicon) was used to detect pimonidazole protein adducts in the tumors. Regions of pimonidazole adducts are stained brown by means of immunoperoxidase second antibody and 3-diaminobenzidine+ chromogen. Five ROIs per tumor slide were digitally photographed at ×200, and positive staining was then quantified with cell^D imaging software and reported as the percentage positive staining per ×200 high-power field. Variations in immunostaining intensity can be seen among the different panels; however, only staining area, not intensity, was considered in the assignment of the quantitative scores for hypoxia.

VEGF-A ELISA of Tumor Lysates and Serum

Snap-frozen tumor tissues were immersed in 400 μL of radioimmunoprecipitation assay buffer before sonification on ice for 20 s. The suspension was separated by centrifugation at 16,000*g* for 10 min. Protein concentrations were determined using a DC protein assay kit (Bio-Rad). Blood was collected by cardiac puncture and kept at room temperature for 2 h, and serum was removed after centrifugation of the samples at 2,000 rpm for 10 min at room temperature in a tabletop cell centrifuge (stored at −80°C).

Levels of VEGF-A in tumor lysates and serum were measured using a human VEGF-A ELISA kit (R&D Systems) according to the manufacturer's instructions and normalized to total protein content for tumor lysates.

Real-Time Quantitative PCR

Total RNA was extracted from tumor tissue and stored in RNAlater, using the RNeasy Mini Kit (Qiagen) according to the manufacturer's instructions. RNA concentration was measured using a NanoDrop 1000 spectrophotometer (Thermo Scientific), and RNA degradation was checked using standard sensitivity chips Experion Software (version 3.0; Bio-Rad). One microgram of total RNA was converted to single-strand complementary DNA by reverse transcription (Superscript; Invitrogen) with Oligo(dT) priming. Complementary DNA was used in real-time quantification with the SYBR green kit (GC Biotech) and 250 nM of each primer. A 2-step program was run on the LightCycler 480 (Roche). Cycling conditions were 95°C for 10 min, 40 cycles of 95°C for 15 s, and 60°C for 1 min. Melting curve analysis confirmed primer specificities. All reactions were run in duplicate and normalized to the geometric mean of human hypoxanthine guaninine phosphoribosyl transferase and succinate dehydrogenase complex, subunit A for the human target genes or normalized to the geometric mean of mouse hypoxanthine guaninine phosphoribosyl transferase and hydroxymethyl-bilane synthase for the mouse target genes. The efficiency of each primer was calculated using a standard curve of reference genomic or complementary DNA (Roche). Amplification efficiency was determined using the formula $10^{-1/\text{slope}}$. For the actual calculations, the base of the exponential amplification function was used (e.g., 2.04 in case of 104% amplification efficiency). Forward and reverse sequences of all reference and target genes are shown in Supplemental Table 2.

Statistical Analysis

Statistical analysis was performed using SPSS software (version 15.0). All data are expressed as mean ± SD. For microSPECT data analysis ($n = 3$ per time group), power analysis was performed as previously described (*7*). Because we could not confirm normal distribution of our data, the less powerful Kruskal–Wallis test for statistical analysis was used. Nonparametric Mann–Whitney testing was performed to assess the significance of the data obtained for both therapy-treated and control data, followed by Bonferroni correction. The Spearman rank correlation *r* was used to calculate the correlations between uptake of ^{99m}Tc-$(CO)_3$ His-annexin A5 and caspase-3–positive cells. Two-sided *P* values of less than 0.05 were considered statistically significant.

RESULTS

Tumor Volumes

Because tumor hypoxia and MVD can vary with tumor size, tumor size (volume) of the control and bevacizumab-treated groups was compared. Tumor volume of control and bevacizumab-treated mice used for all immunohistochemical stainings were 428 ± 27.28 mm^3 (control group, $n = 12$), 477 ± 64.10 mm^3 (bevacizumab day 2, $n = 5$), 512 ±

27.56 mm^3 (bevacizumab day 4, $n = 5$), and 518 ± 37.63 mm^3 (bevacizumab day 6, $n = 5$). No significant difference in tumor volume between the control and bevacizumab-treated mice was observed (Kruskal–Wallis, $P > 0.05$). For the SPECT study, the only significantly different tumor volumes were for the group receiving irinotecan 2 d after the bevacizumab and the baseline group receiving irinotecan 6 d after the bevacizumab (Fig. 1; Kruskal–Wallis, $P < 0.01$). However, to estimate whether partial-volume effect comes into play, we considered the worst-case scenario: an ellipsoidal volume with the long axis twice the short axis and the height. With an average tumor volume of 400 mm^3, the short axis was still 3.6 mm ($8/3\pi \times a^3$, where a equals the short axis and height and long axis equals 2a), whereas the resolution of the novel state-of-the-art micro-SPECT system can reach 450 μm. However, because we used the rat collimator, resolution was in the range of 800 μm to 1 mm—a range still well below partial-volume effect risks.

MVD and Morphology of Tumor Vasculature Modulated by Bevacizumab

The effect of bevacizumab on MVD in tumor tissues of the Colo205 xenograft model was investigated by immunohistochemical staining of vWF. Figure 2A shows the results of the MVD. The number of microvessels positive for vWF was lower in the bevacizumab group than in the control group, and on day 4 MVD was significantly lower ($P < 0.05$) in the bevacizumab group than in the control group.

To identify pericyte coverage of endothelial cells, immunostaining of α-SMA was performed. Compared with the control group, on day 2 and day 4, the fraction of α-SMA–positive cells was higher, although not significant; however, on day 6 the fractions of α-SMA positive cells were significantly lower ($P < 0.01$) (Fig. 2B).

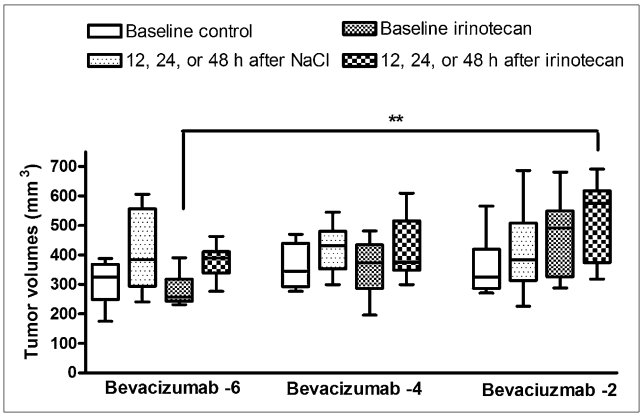

FIGURE 1. Tumor volumes (mm^3) measured at baseline (before therapy) and after therapy at different time points (12, 24, and 48 h) for control and irinotecan-treated mice. Tumor volumes of group receiving irinotecan 2 d after bevacizumab and baseline group receiving irinotecan 6 d after bevacizumab were significantly different (Kruskal–Wallis, $^{**}P < 0.01$).

Masson trichrome staining was performed to detect collagen, a structural component of the vessel wall. On day 2 for the control group, there were many immature vessels, the number of which seemed to decrease on day 4 and day 6. In the bevacizumab group, collagen-covered vessels gradually increased, and on day 6 there was a significant increase ($P < 0.01$), compared with the control group (Fig. 2C). The VMI was calculated as the ratio of α-SMA to vWF staining. A significant increase of VMI was observed on day 2 and day 4; however, this effect had disappeared on day 6, suggesting that even some of the mature vessels were being destroyed (Fig. 2D).

Tumor Hypoxia

Because hypoxia can decrease the efficacy of coadministered chemotherapy, tumor hypoxia after bevacizumab treatment was investigated by pimonidazole staining. On day 2, tumor hypoxia was significantly higher than in time-control tumors ($P < 0.01$) and significantly higher than on day 4 and day 6 ($P < 0.001$). On day 4, tumor hypoxia was lower (although not significantly) than in nontreated control tumors; however, 6 d after single-dose bevacizumab treatment, tumor hypoxia was slightly increased in the bevacizumab-treated tumors, compared with the control tumors (Fig. 2E). Examples of immunostaining of vWF, α-SMA, Masson trichrome, and pimonidazole are shown in Supplemental Figure 1.

Transcription of VEGF-A, Platelet–Endothelial Cell Adhesion Molecule 1 (PECAM-1), α-SMA, and Angiopoietin 1 (Ang-1)

Transcription of VEGF-A slightly decreased on day 2, compared with control tumors, which additionally decreased on day 4. On day 6, transcription of VEGF-A was increased, compared with control tumors, and even slightly higher (Fig. 3A). PECAM-1 and α-SMA, respectively, are molecular markers for endothelial cells and pericytes. Transcription of PECAM-1 was decreased at all time points of bevacizumab treatment, compared with control tumors. Lowest messenger RNA levels of PECAM-1 were observed on day 2, gradually increasing on subsequent days (Fig. 3B). Transcription of α-SMA was investigated, and levels of messenger RNA were all increased, compared with control tumors. The highest transcription level was observed on day 2 and gradually decreased during bevacizumab treatment (Fig. 3C). Ang-1 is known to be involved in recruitment of pericytes in some tumor types; however, neither the control nor the bevacizumab-treated tumors expressed Ang-1 (quantification cycle > 45, data not shown).

Expression of VEGF-A in Tumor Lysates and Serum

Expression level of VEGF-A was measured in the tumors and serum (Figs. 4A and 4B, respectively) by ELISA. Levels of VEGF-A in tumor tissues decreased significantly after a single-dose administration of bevacizumab, compared with the control (Colo205-bearing mice without treatment) at all 3 time-points ($P < 0.05$). In serum, VEGF-A levels were

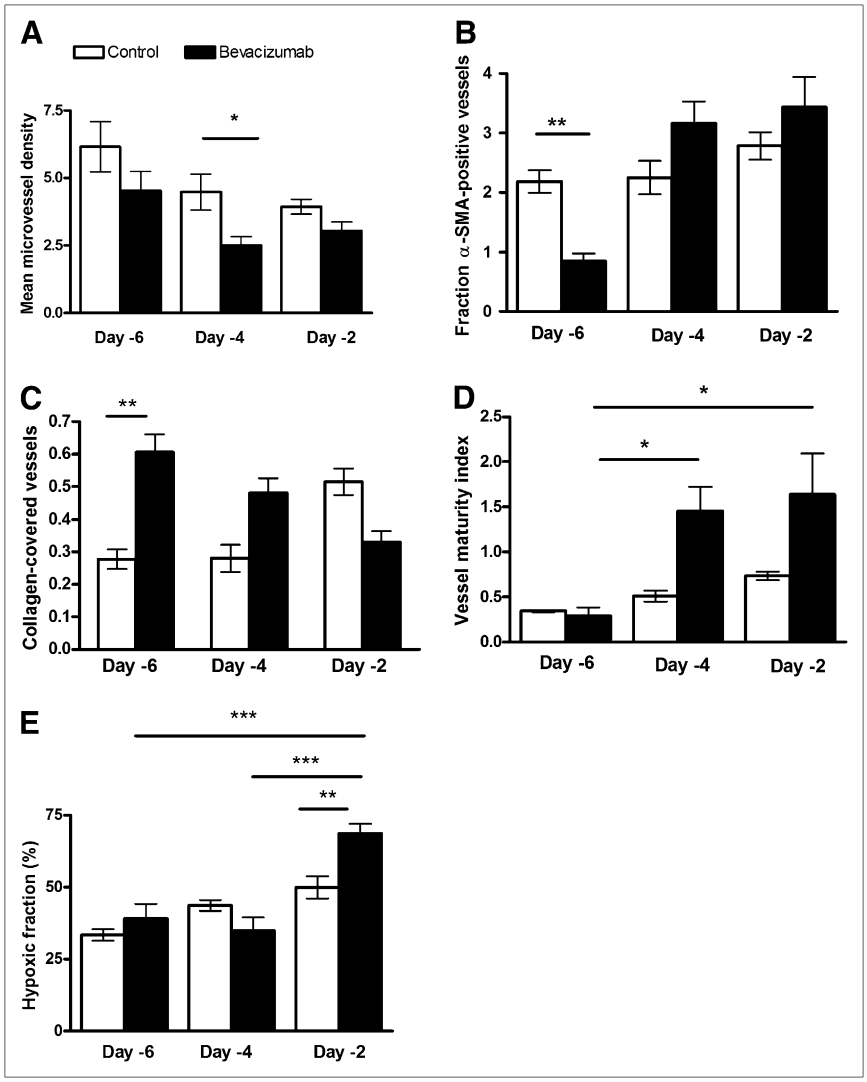

FIGURE 2. Changes in tumor vasculature with bevacizumab treatment in colorectal tumor model. Quantification of MVD (vWF-staining) (A), α-SMA (B), collagen-covered vessels (Masson trichrome staining) (C), VMI (ratio of α-SMA to vWF per tumor section) (D), and hypoxic fraction of bevacizumab-treated (n = 5/time group) and control colorectal tumors (n = 4/time group) (E). $^{*}P < 0.05$. $^{**}P < 0.01$. $^{***}P < 0.001$.

slightly increased, compared with controls, being highest on day 2 and lowest on day 6.

Apoptotic Tumor Response Analyzed by ^{99m}Tc-(CO)$_3$ His-Annexin A5 SPECT and Caspase-3 Immunostaining

The tumor uptake of ^{99m}Tc-(CO)$_3$ His-annexin A5 after treatment with bevacizumab (5 mg/kg) at 2, 4, or 6 d before a single-dose administration of irinotecan (12, 24, and 48 h) is shown in Table 1. Administration of a single dose of bevacizumab 2 d before the irinotecan injection demonstrates a peak of ^{99m}Tc-(CO)$_3$ His-annexin A5 uptake in the tumor at 48 h after irinotecan treatment (162.20 ± 31.20 %ID/g/kg, $P < 0.05$), normalized to controls. Four days after bevacizumab treatment and 24 h after irinotecan treatment, a peak of 232.78 ± 24.82 %ID/g/kg ($P < 0.05$) in ^{99m}Tc-(CO)$_3$ His-annexin A5 uptake in the tumor was observed. However, only a small increase in tumoral uptake of the radiotracer was measured (109.52 ± 29.81 %ID/g/kg) 6 d after bevacizumab treatment and 48 h after irinotecan administration.

To confirm the presence of apoptotic cells in the tumors, caspase-3 staining was performed on all tumor slides. The values of caspase-3–positive immunostaining in treated tumors, over controls, are shown in Table 2. A large peak of caspase-3–positive cells was observed 4 d after bevacizumab treatment and 24 h after irinotecan treatment (185.87% ± 24.64%, $P < 0.05$) and a second, smaller peak when bevacizumab was administered 2 d before the irinotecan injection at 48 h (124.21% ± 19.21%). Correlation analysis (Spearman rank) between the parameters ^{99m}Tc-(CO)$_3$ His-annexin A5 uptake in the tumor and percentage caspase-3–positive cells revealed a correlation (R^2) of 0.8119 ($P = 0.04$). Immunostaining for caspase-3 is shown in Supplemental Figure 2. Representative SPECT images of control and treated tumors are shown in Figure 5.

DISCUSSION

For chemotherapy to be effective, it must be delivered in sufficiently high concentrations into the tumor. In this manner, chemotherapy can exert its cytotoxic effects by

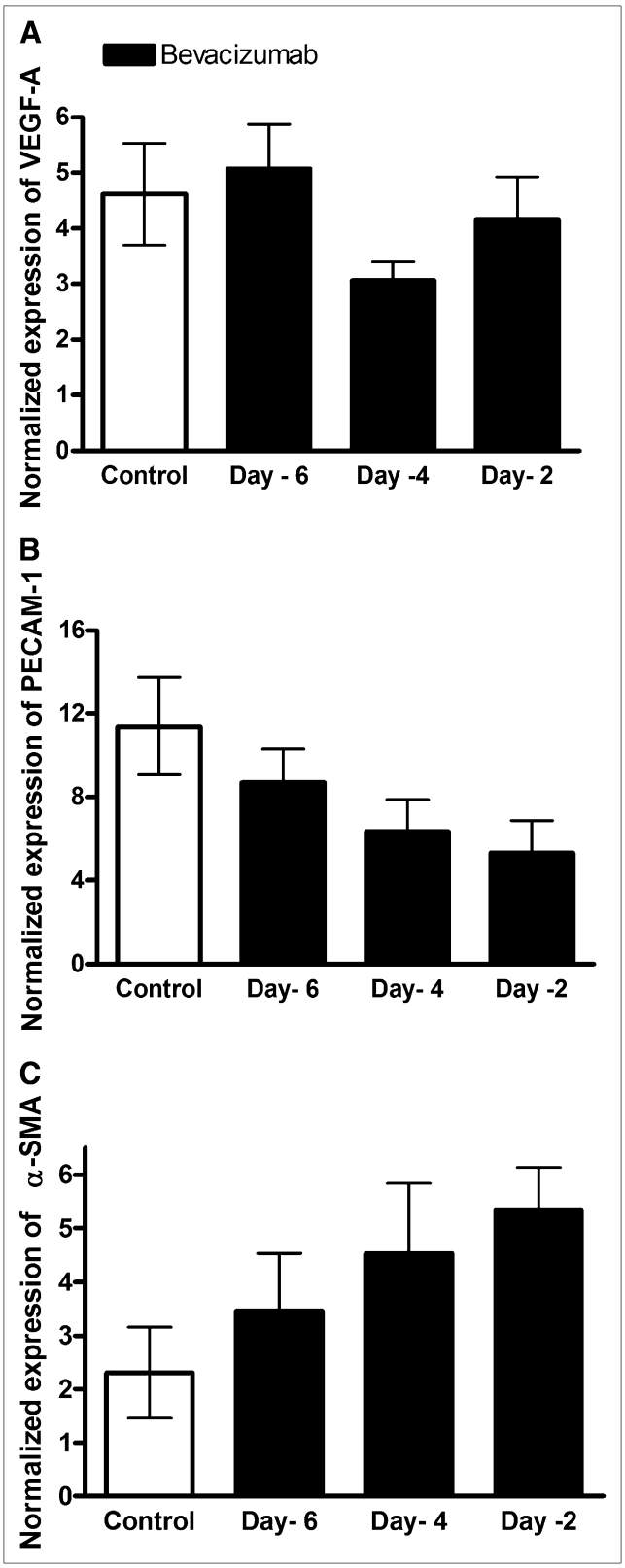

FIGURE 3. Messenger RNA expression of human VEGF-A (A), mouse PECAM-1 (B), and mouse α-SMA (C). Data are normalized to human (VEGF) or mouse housekeeping genes (α-SMA and PECAM-1).

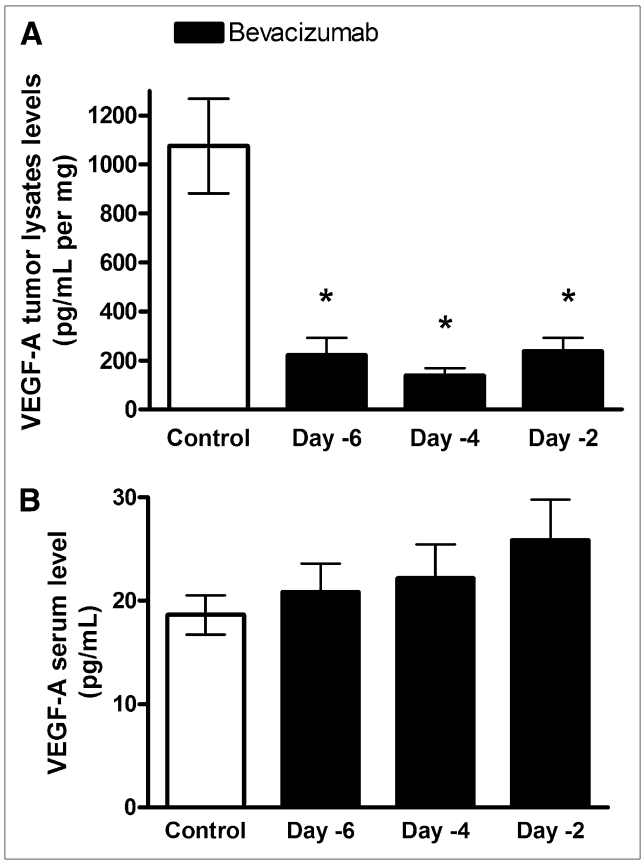

FIGURE 4. Levels of VEGF-A were measured by ELISA in tumor lysates (A) and serum samples (B). *$P < 0.05$.

inducing cell death of the malignant tumor cells. However, the aberrant tumoral vessel structure and the chaotic tumor blood supply may hamper efficient drug delivery. Transient normalization of the tumor vessel structure by antiangiogenic drugs such as bevacizumab may improve vascular function and as a result improve delivery and efficacy of coadministered chemotherapy. In our colorectal tumor model, we investigated the alterations in tumor vessel density, tumor vessel morphology, and tumor oxygenation induced by a single-dose treatment with the anti-VEGF antibody bevacizumab. Next, a single dose of irinotecan was administered on different days after bevacizumab treatment, and the efficacy of irinotecan in inducing cell death in the tumor was investigated by radiolabeled annexin A5 SPECT and compared with caspase-3 immunostaining. The imaging of apoptosis noninvasively by radiolabeled annexin A5 has already been proven to be an excellent tool for the detection of apoptosis induced by chemoradiotherapy (*9–11*). Moreover, a noninvasive way to detect the extent and timing at which therapeutic regimen–dependent apoptosis occurs may provide clinicians with relevant information on disease activity and therapeutic efficacy.

Bevacizumab clearly decreases MVD in our model, with a significant decrease found on day 4 after administration of a single dose of bevacizumab. At the same time, more blood vessels are covered by pericytes (increased α-SMA–

TABLE 1
^{99m}Tc-$(CO)_3$ His-annexin A5 Uptake in Tumors

	Time after NaCl or irinotecan treatment (h) (n = 3)					
	12		24		48	
Bevacizumab at...	NaCl	Irinotecan	NaCl	Irinotecan	NaCl	Irinotecan
2 d	81.55 ± 4.63	102.76 ± 11.09	103.70 ± 31.31	92.43 ± 7.77	104.26 ± 30.25	162.20 ± 31.20*
4 d	76.76 ± 19.60	77.15 ± 19.51	71.31 ± 9.52	232.78 ± 24.82**	79.74 ± 17.61	117.05 ± 28.70
6 d	73.93 ± 16.53	76.36 ± 27.78	97.29 ± 18.90	126.94 ± 20.71	102.50 ± 29.63	109.52 ± 29.81

*$P < 0.05$.
Data are expressed as %ID/tumor weight (g)/body weight (kg) and normalized to controls (n = 9) and are mean ± SD.

positive vessels) and surrounded by collagen (indicated by Masson trichrome staining). The ratio between α-SMA and vWF, a quantitative marker of vessel maturity, is significantly increased by bevacizumab on days 2 and 4 after the start of the treatment. All these observations suggest a morphologic normalization of the tumor vasculature, especially on day 4. In addition, on day 6 VMI was decreased significantly, suggesting that this normalization is a transient process. Vessel normalization induced by antiangiogenic therapy has already been suggested in various animal models and human patients (*12–14*).

To investigate whether this morphologic normalization of the tumor vasculature is accompanied by enhanced drug delivery, a single dose of irinotecan was administered after treatment with bevacizumab for 2, 4, or 6 d. A previous study of our research group in the same model demonstrated a peak in tumoral ^{99m}Tc-$(CO)_3$ His-annexin A5 uptake (163 ± 13 %ID/g/kg) 24 h after treatment with a single dose of irinotecan (100 mg/kg), normalized to controls; however, treatment with a single dose of bevacizumab (5 mg/kg) did not increase uptake of the radiotracer (*7*). On day 2, a peak in ^{99m}Tc-$(CO)_3$ His-annexin A5 uptake in the tumor was observed, 48 h after irinotecan administration (162.20 ± 31.20 %ID/g/kg). At that moment, VMI was increased, suggesting a normalization of the tumor vasculature; however, tumor hypoxia was also increased. Hypoxic tumors are characterized by an increased resistance to cytotoxic agents (*15*). In conclusion, although on day 2 a normalization of the vasculature is suggested by our data, the high hypoxic environment hinders a better killing efficiency of the irinotecan. On day 4, a high VMI and a low hypoxic tumor background resulted in a significant peak in ^{99m}Tc-$(CO)_3$ His-annexin A5 uptake in the tumor 24 h after irinotecan administration (232.78 ± 24.82 %ID/g/kg). The observed normalization of the tumor vasculature, including the increased collagen around the tumor vessels, suggests a better drug delivery of the irinotecan in the tumor, followed by a more efficient cytotoxic effect of the drug. In fact, the observed peak of 232.78 ± 24.82 % ID/g/kg ^{99m}Tc-(CO_3) His-annexin A5 is about 60%–70% higher than with the monotherapy treatment, suggesting a synergistic induction of apoptosis by bevacizumab and irinotecan. On day 6, mean MVD increases slightly (however, it is still lower when compared with the control group), and collagen-covered vessels increase significantly. VMI on day 6 was significantly lower than on days 2 and 4, suggesting that the normalization window has passed. Only a small level of ^{99m}Tc-$(CO)_3$ His-annexin A5 uptake in the tumor 24 h after irinotecan administration (109.52 ± 29.81 %ID/g/kg) was observed. Conceivably, the tumor vessels at this moment show an abnormally thick basement membrane, indicated by the high number of collagen-covered vessels, which may impair efficient irinotecan delivery in the tumor. Ex vivo imunohistochemical staining of caspase-3 (apoptotic marker) of the tumor slides confirmed the observed peaks in ^{99m}Tc-$(CO)_3$ His-annexin A5 uptake

TABLE 2
Caspase-3–Positive Cells in Tumors

	Time after NaCl or irinotecan treatment (h) (n = 3)					
	12		24		48	
Bevacizumab at...	NaCl	Irinotecan	NaCl	Irinotecan	NaCl	Irinotecan
2 d	62.21 ± 11.31	63.91 ± 8.91	94.46 ± 13.97	86.59 ± 22.48	72.29 ± 4.92	124.21 ± 19.21
4 d	51.60 ± 17.87	89.74 ± 4.73	62.32 ± 14.74	185.76 ± 24.64**	52.98 ± 4.46	104.38 ± 10.90
6 d	68.20 ± 8.05	87.72 ± 20.42	56.43 ± 16.17	113.50 ± 8.52	85.92 ± 15.98	104.85 ± 20.72

*$P < 0.05$.
Data are expressed as percentage caspase-3–positive cells and normalized to controls (n = 9) and are mean ± SD.

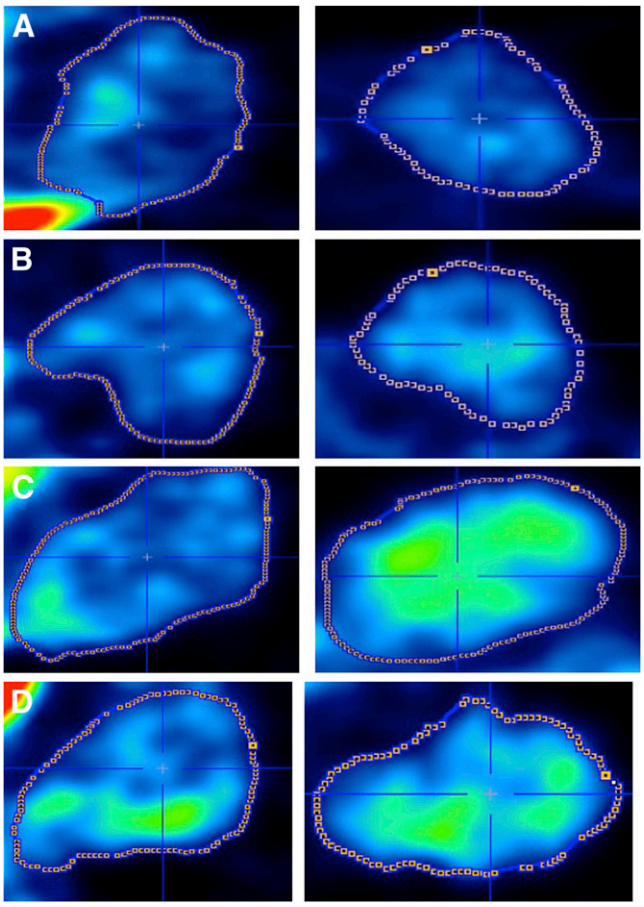

FIGURE 5. Micro-SPECT images of Colo205 tumors at 3.5 h after injection of 18.5 MBq of ^{99m}Tc-$(CO)_3$ His-Annexin A5 in tail vein. Mice received 0.9% NaCl for 12 h (A, left) or for 24 h (A, right) before administration of radiotracer, bevacizumab (5 mg/kg) 6 d before 0.9% NaCl for 24 h (B, left) or irinotecan (100 mg/kg) for 48 h (B, right), bevacizumab 4 d before 0.9% NaCl for 24 h (C, left) or irinotecan for 24 h (C, right), and bevacizumab 2 d before 0.9% NaCl for 48 h (D, left) or irinotecan for 48 h (D, right). Representative sagittal slices demonstrate accumulation of ^{99m}Tc-$(CO)_3$ His-Annexin A5 in tumors.

in the tumor ($R^2 = 0.8119$, $P < 0.05$). Several other studies have investigated the efficacy of anti-VEGF therapy and coadministered chemotherapy. Higher tumor CPT-11 (or irinotecan) concentrations were also found in a HT-29 colorectal cancer model, when mice were treated twice (days 0 and 4) with the anti-VEGF antibody A4.6.1 (*16*). In a murine mammary carcinoma model, treatment of the mice with a single dose of anti-VEGF antibody DC101 resulted 3 d later in a normalization of the tumor vasculature (*17*). In an orthotopic neuroblastoma model, penetration of chemotherapy was improved by as much as 81% when given 1–3 d after bevacizumab, compared with when drugs were given concomitantly or 7 d apart (*18*). Ang-1 is known to have clear effects on the vasculature because it has been shown to be involved in recruitment of pericytes, facilitating the interaction between endothelial cells and pericytes during angiogenesis (*19*). In a glioma tumor model, Ang-1 was significantly upregulated by cancer cells on days 2 and 5 (peak of pericyte coverage) after DC101 therapy, but not on day 1 or day 8 (*20*). In our colorectal model, no expression of Ang-1 in the tumors was observed at any time points, perhaps suggesting that this protein is not (or is less) involved in the recruitment of pericytes in colorectal cancers.

Bevacizumab captures free human VEGF-A (and with lower-affinity VEGF of other species), blocking the binding of VEGF-A to the VEGF-A receptors expressed on vascular endothelial cells and tumor cells. High levels of VEGF-A messenger RNA were detected in control and bevacizumab-treated animals. However, on day 4 after the start of the bevacizumab treatment, transcription of VEGF-A decreased, although not significantly, compared with control tumors. At all time points, VEGF-A levels determined in the tumors by ELISA were significantly decreased, compared with control tumors. Treatment with bevacizumab seems not to affect transcription of the VEGF-A gene, whereas VEGF-A protein levels were significantly decreased in tumor, confirming the working mechanism of the VEGF antibody. In the serum, VEGF-A levels are slightly increased on day 2 after bevacizumab treatment, compared with control animals, and return to control levels on day 6.

CONCLUSION

Overall, we found a supraadditive effect from bevacizumab treatment given 4 d before irinotecan was administered. Knowledge of the time window during which tumoral vessels become normalized is essential. When chemotherapy was given outside this window, no therapeutic effect was seen. The ability to measure chemotherapy-induced cell death noninvasively may help clinicians to determine the most optimal combination treatment schedule of anti-VEGF treatment and chemotherapy.

DISCLOSURE STATEMENT

The costs of publication of this article were defrayed in part by the payment of page charges. Therefore, and solely to indicate this fact, this article is hereby marked "advertisement" in accordance with 18 USC section 1734.

ACKNOWLEDGMENTS

We express our gratitude to Philippe Joye for his assistance in animal handling and Steven Deleye for his technical assistance in handling the U-SPECT-II. Part of this work was financially supported by the European Union through the grant Euregional PACT II by the Interreg IV program of Grensregio Vlaanderen-Nederland (IVA-VLANED-1.20). No other potential conflict of interest relevant to this article was reported.

REFERENCES

1. Presta LG, Chen H, O'Conner SJ, et al. Humanization of an anti-vascular endothelial growth factor monoclonal antibody for the therapy of solid tumors and other disorders. *Cancer Res*. 1997;57:4593–4599.
2. Tonra JR, Hicklin DJ. Targeting the vascular endothelial growth factor pathway in the treatment of human malignancy. *Immunol Invest*. 2007;36:3–23.

3. Hurwitz H, Fehrenbacher L, Novotny W, et al. Bevacizumab plus irinotecan, fluorouracil and leucovorin for metastatic colorectal cancer. *N Engl J Med*. 2004;350:2335–2342.
4. Carmeliet P, Jain RK. Angiogenesis in cancer and other diseases. *Nature*. 2000;407:249–257.
5. Jain RK. Normalization of tumor vasculature: an emerging concept in antiangiogenic therapy. *Science*. 2005;307:58–62.
6. Vangestel C, Peeters M, Oltenfreiter R, et al. In vitro and in vivo evaluation of [^{99m}Tc]-labeled tricarbonyl His-annexin A5 as an imaging agent for the detection of phosphatidylserine-expressing cells. *Nucl Med Biol*. 2010;37:965–975.
7. Vangestel C, Van de Wiele C, Mees G, et al. SPECT imaging of the early time course of therapy-induced cell death using ^{99m}Tc-(CO)3 His-annexin A5 in a colorectal cancer xenograft model. *Mol Imaging*. In press.
8. van der Have F, Vastenhouw B, Ramakers RM, et al. U-SPECT-II: an ultra-high-resolution device for molecular small-animal imaging. *J Nucl Med*. 2009;50:599–605.
9. Blankenberg FG, Katsikis PD, Tait JF, et al. Imaging of apoptosis (programmed cell death) with ^{99m}Tc annexin V. *J Nucl Med*. 1999;40:184–191.
10. Ohtsuki K, Akashi K, Aoka Y, et al. Technetium-^{99m}HYNIC-annexin V: a potential for the in-vivo detection of apoptosis. *Eur J Nucl Med Mol Imaging*. 1999;26:1251–1258.
11. Subbarayan M, Häfeli UO, Feyes DK, Unnithan J, Emancipator SN, Mukhtar H. A simplified method for preparation of ^{99m}Tc-annexin V and its biological evaluation for in vivo imaging of apoptosis after photodynamic therapy. *J Nucl Med*. 2003;44:650–656.
12. Myers AL, Williams RF, Ng CY, Hartwich JE, Davidoff AM. Bevacizumab-induced tumor vessel remodelling in rhabdomyosarcoma xenografts increases the effectiveness of adjuvant ionizing radiation. *J Pediatr Surg*. 2010;45:1080–1085.
13. Huang G, Chen L. Recombinant human endostatin improves anti-tumor efficacy of paclitaxel by normalizing tumor vasculature in Lewis lung carcinoma. *J Cancer Res Clin Oncol*. 2010;136:1201–1211.
14. Willett CG, Boucher Y, di Tomaso E, et al. Direct evidence that the VEGF-specific antibody bevacizumab has antivascular effects in human rectal cancer. *Nat Med*. 2004;10:145–147.
15. Teicher BA. Hypoxia and drug resistance. *Cancer Metastasis Rev*. 1994;13:139–168.
16. Wildiers H, Guetens G, De Boeck G, et al. Effect of antivascular endothelial growth factor treatment on the intratumoral uptake of CPT-11. *Br J Cancer*. 2003;88:1979–1986.
17. Tong RT, Boucher Y, Kozin SV, Winkler F, Hicklin DJ, Jain RK. Vascular normalization by vascular endothelial growth factor receptor 2 blockade induces a pressure gradient across the vasculature and improves drug penetration in tumors. *Cancer Res*. 2004;64:3731–3736.
18. Dickson PV, Hamner JB, Sims TL, et al. Bevacizumab-induced transient remodelling of the vasculature in neuroblastoma xenograft results in improved delivery and efficacy of systemically administered chemotherapy. *Clin Cancer Res*. 2007;13:3942–3950.
19. Jain RK. Molecular regulation of vessel maturation. *Nat Med*. 2003;9:685–693.
20. Winkler F, Kozin SV, Tong RT, et al. Kinetics of vascular normalization by VEGFR2 blockade governs brain tumor response to radiation: role of oxygenation, angiopoetin-1 and matrix metalloproteinases. *Cancer Cell*. 2004;6:553–563.